Modelling the interphase of 3D printed photo-cured polymers

Lorenzo De Noni[1], Laura Zorzetto[2,3], Francesco Briatico-Vangosa[1], Marta Rink[1], Davide Ruffoni[3], Luca Andena[1,*]

1 Dipartimento di Chimica, materiali e ingegneria chimica “G. Natta", Politecnico di Milano, Milan, Italy

2 Max Planck Institute of Colloids and Interfaces, Department of Biomaterials, Am Mühlenberg 1 - 14476 Potsdam, Germany

3 Mechanics of Biological and Bioinspired Materials Laboratory, Department of Aerospace and Mechanical Engineering, University of Liège, Liège, Belgium

* Corresponding Author:

Luca Andena

Dipartimento di Chimica, materiali e ingegneria chimica «G. Natta »

Politecnico di Milano, piazza Leonardo da Vinci 32

20133 Milano, Italy

E-mail: luca.andena@polimi.it

Abstract

3D printing, in particular the Polyjet technology, has been widely employed for the production of complex heterogeneous composites such as co-continuous architectures (the so-called Interpenetrating Phase Composites, IPCs). It is a manufacturing method in which discrete photopolymer droplets of different materials can be deposited on a build tray and cured by UV light lamp. Previous research already demonstrated how the characteristics of the interface between different photopolymers can vary if formed before or after UV curing process. In the first case, droplets of different photopolymers are deposited within the same layer and come into contact before polymerization. In the second scenario, droplets land on a previously deposited layer of a different material after its (partial) curing. In the present work, the dynamic-mechanical properties of multilayer bimaterial composites were investigated using a tensile loading configuration, which is relatively insensitive to the spatial arrangement of layers, as opposed to a bending configuration. This advantage allowed the development of a simple analytical model which incorporates the properties of the two photopolymers and their interphase, which could be used to better represent the actual behaviour of real co-continuous architectures as obtained by Polyjet printing.

Keywords: 3D printing, Polyjet technique, interphase, dynamic mechanical analysis (DMA)

1 Introduction

Three-dimensional (3D) printing is traditionally used to prototype new design concepts and to build layer-by-layer the desired component. It is commonly employed for the production of complex structures and to develop heterogeneous composites with tight control on the local microstructure and material composition [1–3]. Hence, in contrast with the more common subtractive techniques, which involve removing sections of material by cutting or machining it away, 3D printing consists in the addition of material layers to obtain the end-product. There is a lot of ongoing research aimed at improving the final characteristics of 3D printed objects acting on material formulation or on the optimization of printing process and parameters [4].

Among the many available techniques, Polyjet-based manufacturing is attracting a lot of interest since it allows the production of complex architectures by employing more than one material at the same time, whose properties can be widely different: for instance, a hard, glassy polymer coupled with a soft, rubbery one, with elastic moduli at room temperature differing by about three orders of magnitude. This feature has been recently exploited by several authors to produce bio-inspired composite materials [1,5–12]. Briefly, Polyjet 3D printing is a layer-by-layer method where one or more photo-curable liquid polymers are jetted in the form of droplets through several printing nozzles onto a build tray [1]. If necessary, a removable support material can sustain the deposited material to build overhanging features; then, a "levelling roller" immediately removes the excess of material on each pass of the inkjet head and subsequently a curing process is performed with UV lamps to harden each layer, as shown in Figure 1. Currently, such technique allows an in-plane resolution of about 40 μm.

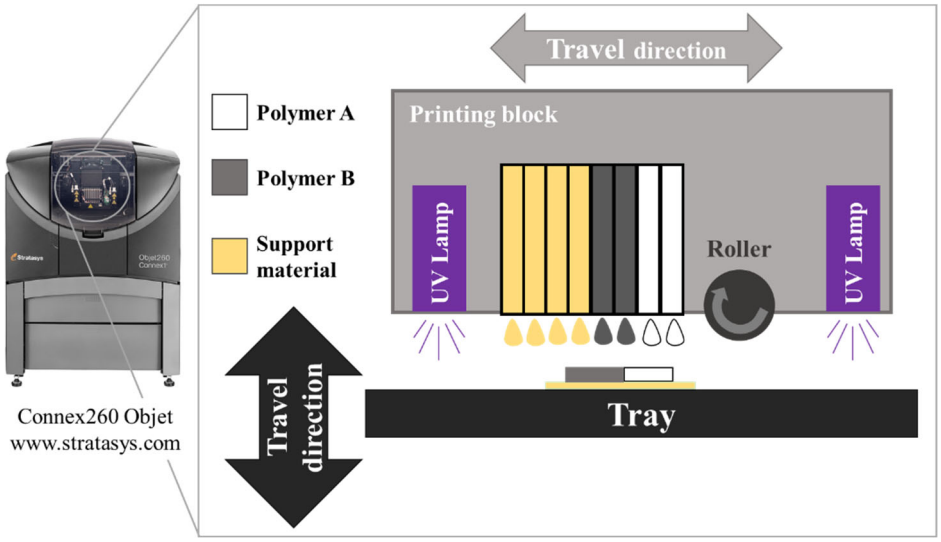

Figure 1. Schematic overview of the 3D Polyjet technology with the main features of the printing process.

Polyjet printing enables to combine different materials and structures to manufacture a large variety of components: for example, blends, also referred to as "digital materials", with intermediate mechanical behaviour with respect to that of constituent materials [13,14]. Even more complex architectures, such as interpenetrating phase composites (IPCs), can be easily built [15]. IPCs are defined as "*two phases or more that are interconnected in three dimensions and construct a topologically continuous network throughout the microstructure*" [16]. Triply periodic minimal surfaces (TPMS) are a class of IPCs becoming more and more popular as minimal interface structures may enhance multifunctional aspects of composites [17–20]. Many experimental and numerical studies have shown how IPCs can be finely tuned to obtain final mechanical properties within a broad range.

Most of these studies implicitly assume that an ideal, zero-thickness interface exists between different phases of multimaterial composites [21,22]. However, several previous works demonstrated that the characteristics of the interface are highly critical for the overall composite behaviour [23–28]. Considering Polyjet printing, interface properties can vary significantly, depending on whether droplets of the different liquid photo-polymers get in contact either before or after the UV curing process. The former case occurs when the two liquid materials are simultaneously deposited on the printing tray, the latter when a given layer is deposited onto an already partially cured one made of a different photo-polymer. During simultaneous deposition, interdiffusion between the two polymers can give rise to a broad, "blurred" interface [23–25,28–30], whose spatial extent is far from being negligible (about 150 μm according to [23]). In the other case, when the second polymer is jetted on an already (at least partially) cured one, the interface is significantly sharper (less than 20-25 μm) [23,30] and actually narrower than the typical in-plane resolution of Polyjet printers (i.e., about 40 μm). In both cases, the layer which forms at the interface between stiff and compliant materials has a finite thickness and will be referred in this work as interphase, to highlight the blending of the two polymers and the possible formation of an effective third material with intermediate properties.

Interphase characteristics can be controlled by changing the layer arrangement in multi-layered composites and by modifying the printing direction. This possibility was exploited in [23] by producing composites having different configurations of stiff and compliant layers, that were later tested using nanoindentation and dynamic-mechanical analysis (DMA) to determine interphase width and macroscopic mechanical response. The study also highlighted a pivotal impact of the interphase on the load transfer between stiff and compliant layers. However, the choice of the most typical (at least for rigid plastics) DMA configuration, i.e. bending, introduced an additional degree of complication because the results were influenced by the spatial arrangement of the layers: those situated farther from the bending neutral axis obviously gave a much higher relative contribution. For this reason, bending-based DMA testing did not allow a straightforward characterization of the dynamic moduli of the interphase.

To overcome this limitation, the main aim of the present work is to develop and validate a model that accounts for the presence of a third interphase between the two main polymer constituents. A simpler DMA tensile testing configuration was selected, with the obvious advantage that in tension a uniform loading strain is applied, thus allowing for a direct identification of the unknown interphase properties using simple parallel/series combinations.

2 Materials and methods

2.1 Sample preparation

The same two base materials (VeroWhitePlus, VW+ and TangoBlackPlus, TB+) and 3D printer (Objet 260, Stratasys, US) described in [23] were employed in the present study. Sample fabrication was performed according to the same printing setup and following the same experimental procedures detailed in our previous work. Briefly, samples were fabricated with the digital material option of the 3D printer allowing for a resolution of 600 x 300 x 800 dots per inch (DPI) along the x, y, and z direction, respectively. A glossy surface finish was used and support material was gently removed with a metal scraper. Up to 3 samples were manufactured simultaneously on the build tray, always at the same position. Sample manufacturing and storage were conducted in a laboratory with constant temperature and humidity. Since the (unknown) composition of the constituent materials is potentially subject to changes by the manufacturer at any time, base materials and composite samples were printed anew using single new batches of supplies from the producer.

Plate-like composite samples, all having 50-50 composition of VW+/TB+, were fabricated by stacking alternating layers of the two materials along their thickness (AT) or width (AW) as depicted in Figure 2 (on the left and on the right, respectively). Samples were designed to evaluate the role of different interphase type (e.g. sharp or blurred) and arrangement on their macroscopic tensile properties: they were all 3D printed in

such a way that during tensile testing a parallel configuration, with identical axial deformation on each layer and a total load equal to the sum over the layer sequence, is realized. However, as already mentioned in [23], each sample type can be produced using two different printing setups: horizontal (Figure 2b-2d) and vertical (Figure 2a-2c). For a given configuration, each printing orientation is associated to the presence of a specific type of interphase (sharp or blurred) between the two jetted polymers.

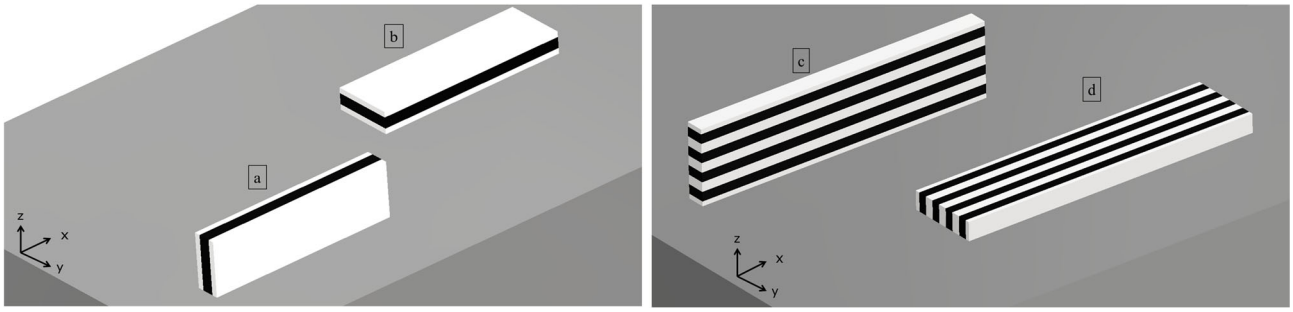

Figure 2. Sketch of sample configurations: layers are stacked symmetrically on the left along the thickness (AT with 2 layers) and on the right along the width (AW with 8 layers). Each sample configuration can be printed according to vertical (*a, c*) or horizontal (*b, d*) orientation.

Nominal sample dimensions were about 1 mm in thickness, 5.1-5.4 mm in width (depending on printing orientation) and 40 mm of gauge length. These values were chosen based on printer's resolution, number of layers and compatibility with DMA testing setup. The rigid VW+ material was always placed at the outer layers, to provide a continuous, firm gripping surface. The whole set of specimens was designed to be symmetric with respect to their mid-plane in order to avoid in-plane bending coupling. Accordingly, multi-layered samples always have a central TB+ layer and two outer semi-layers having each half the thickness of the inner ones, so that the nominal volume of the two basic phases remains equal. Additionally, homogeneous samples made of the pure VW+ and TB+ constituent materials were also prepared to obtain reference data. All samples were produced with two extra gripping regions, having each a length of 15 mm and always made of VW+, located at the opposite ends along the major axis (not shown in Figure 2).

For composite samples, the number of layers was varied while keeping constant the relative volume fractions of WV+ and TB+. Figure 3 summarizes the nominal thickness of the inner layers corresponding to each printed configuration (the two outer layers had always half the listed thickness). The interphase thickness was assumed equal to 20 and 150 micrometres, based on nanoindentation results [23] for sharp and blurred scenarios, respectively. The volumetric fraction of the interphase was estimated accordingly for each configuration (AT or AW), number of layers and printing orientation (horizontal or vertical); relevant values are reported in Figure 4. Printing of AT vertical samples with more than 4 layers proved unsuccessful, since the final geometry obtained was not sufficiently accurate in this case.

Finally, the effect of the relative content of the two constituents (VW+ and TB+) was investigated by producing modified 2-layers AT samples (horizontally printed) whose central TB+ layer had increasing thickness corresponding to the following nominal (i.e. without considering the interphase) volume fractions of this constituent: 50% (standard, according to Figure 3); 62.5%; 75%; 87.5%; 92%; 95%. All samples were produced in triplicates after calibrating the UV lamp to guarantee consistency of the curing process.

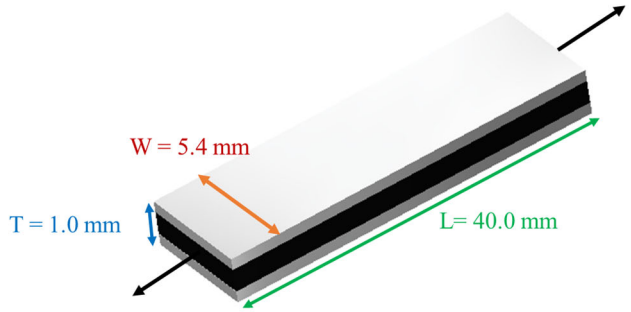

# of layers	2	4	8	16	32
AT horizontal	0.500	0.250	0.125	-	-
AW horizontal	-	-	0.680	0.340	0.170
AW vertical			0.640	0.320	0.160

Figure 3. AT sample with 2 layers where the relevant dimensions (in mm) are specified and arrows indicate the loading condition (on the left); layer thickness (in mm) as a function of sample configuration and number of layers (table on the right).

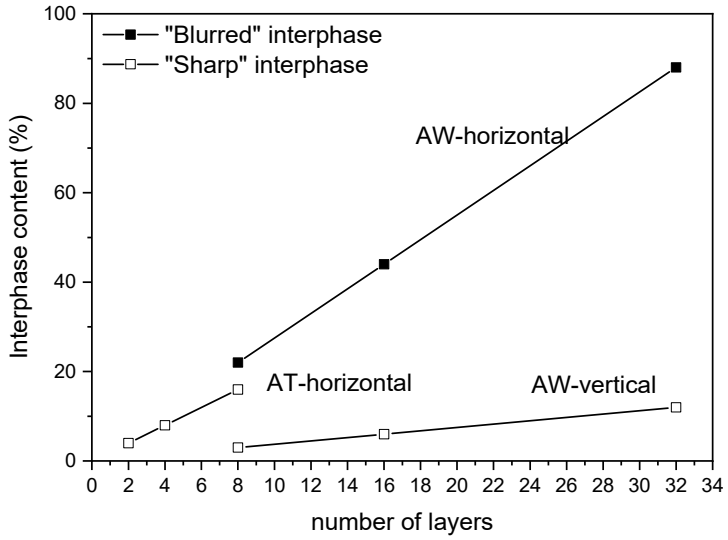

Figure 4. Volumetric content of the interphase as a function of the sample configuration and printing direction: solid symbols refer to "blurred" interphase, whereas hollow symbols to "sharp" interphase.

2.2 Dynamic mechanical analysis (DMA)

Dynamic mechanical analysis was carried out in tensile configuration with a RSA III Rheometrics System Analyzer (TA Instruments, US). A temperature ramp was applied to measure the response in terms of storage modulus, *E'*, and of the major thermal transitions as detected by identifying the main peaks in the loss factor vs. temperature curves. The same heating rate (5 °C/min) used in [23] was applied, but the temperature range was extended in both directions to allow for completion of the glass transitions therein reported. Samples were first cooled from room temperature to -50 °C, stabilized for at least 5 minutes, and subsequently heated up to 80 °C. An oscillatory displacement resulting in 0.1% strain was applied along the main sample axis to keep the material within the linear viscoelastic regime; the selected frequency was 1 Hz, in agreement with our previous analysis [23]. Dynamic pre-tensioning of the sample was employed, adjusting the static force to 20% of the measured dynamic one to prevent complete unloading during the applied strain cycle. Force and phase angle data were collected every 12 seconds (i.e. every 1°C). For each configuration, three samples were tested and results were averaged.

3 Preliminary tests

It is well known that many process parameters may affect the final properties of polymeric components, and this is true also for 3D-printed parts. In this section results of preliminary testing concerning curing conditions and layer stacking are reported before moving on to the main objective of the investigation, to confirm the validity of the chosen approach.

3.1 Effect of curing conditions

While exploring a broader temperature range with respect to our previous research [23], we observed some discrepancies in the data at high temperature obtained on supposedly identical samples. We attributed this unexpected variability to a non-uniform degree of crosslinking of the VW+ phase in the newly printed samples. If the amount of UV radiation is not sufficient to ensure complete crosslinking, some variations may arise depending on the sample positioning on the printing tray. To confirm this hypothesis, we performed consecutive DMA scans interspersed by cooling cycles, always up to 80°C as described in the previous section. A typical result of the comparison between the first two scans on the same VW+ sample is displayed in Figure 5.

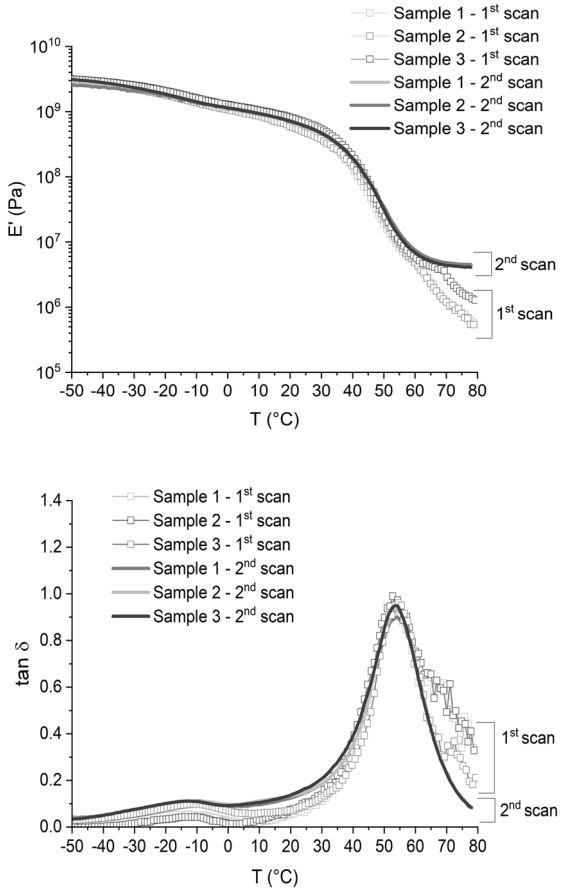

Figure 5. Storage modulus (top) and loss factor (bottom) curves for horizontally printed AT samples with 2 layers: first scan (open square); second scan (continuous lines). The graphs also show an example of data repeatability (three samples) under same test conditions.

The behaviour in the region above 60°C is markedly different for the two scans. On the first one, *E'* data shows a continuously decreasing trend even above the reported glass transition of 54°C for VW+ [23]. On the second run, a typical rubbery plateau is observed instead. Subsequent scans performed on the same samples produce data identical to the second one, and a very good repeatability of the data can be observed. This behaviour is common for all samples whose mechanical response depends on the presence of the VW+ phase. The proposed interpretation is that standard curing conditions enforced by the Objet 260 printer do not ensure complete

crosslinking of the VW+ component, which is instead achieved by heating the sample up to 80°C thereafter. Accordingly, a preliminary DMA scan was applied to all samples to make sure they were in the same state before actual testing. Results reported from now on belong to the 2nd scan performed on each sample.

3.2 Effect of layer stacking sequence

To verify the independence of obtained results from the arrangement of the two constituent materials, the mechanical behaviour of samples having VW+ or TB+ in the two outer semi-layers was compared. Results shown in Figure 6 demonstrate how switching the two materials produces no effect even when only 2 layers (or, better, a single layer and two semi-layers) are present. This is by far the situation in which a possible influence of the spatial arrangement of the two materials with respect to the mid-section would be more easily identified and, accordingly, this scenario was not further considered.

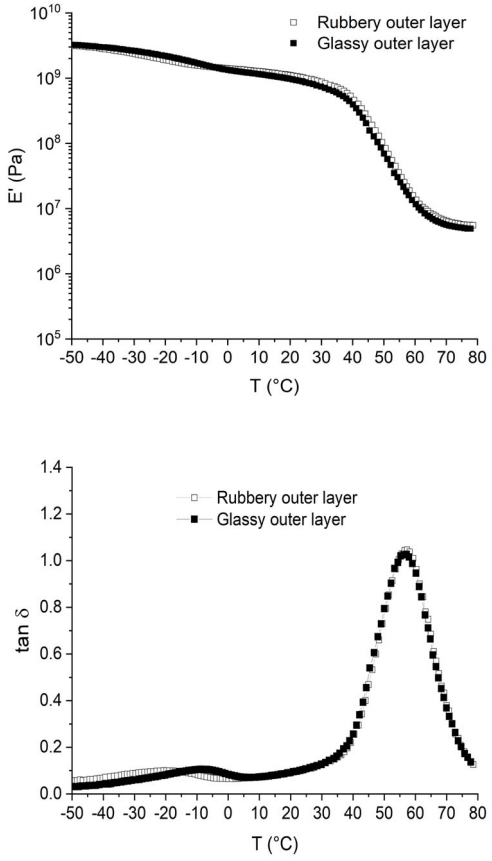

Figure 6. Storage modulus (top) and loss factor (bottom) of a standard "horizontally"-printed 2-layer AT sample (VW+ outside, TB+ inside) and its counterpart with switched constituents.

4. Results and discussion

Moving now to the main findings, Figure 7 shows results obtained on the two pure materials, VW+ and TB+. VW+ has a glass transition temperature of approximately 59 °C, across which the measured storage modulus decreases from the glassy plateau approximately at 3.5 GPa to the high-temperature rubbery plateau at about 10 MPa. In contrast, neat TB+ displays a glass transition temperature approximately at 6 °C across which the storage modulus is decreasing from 3 GPa to less than 1 MPa. It is worth noting that a single main peak can be detected in the loss factor curve of TB+. Other works based on DMA in tensile or compressive configurations also reported a single peak for similar rubbery constituents but at slightly lower temperature (-5 °C for TangoBlack [31] and -1 °C for Tango [32]).

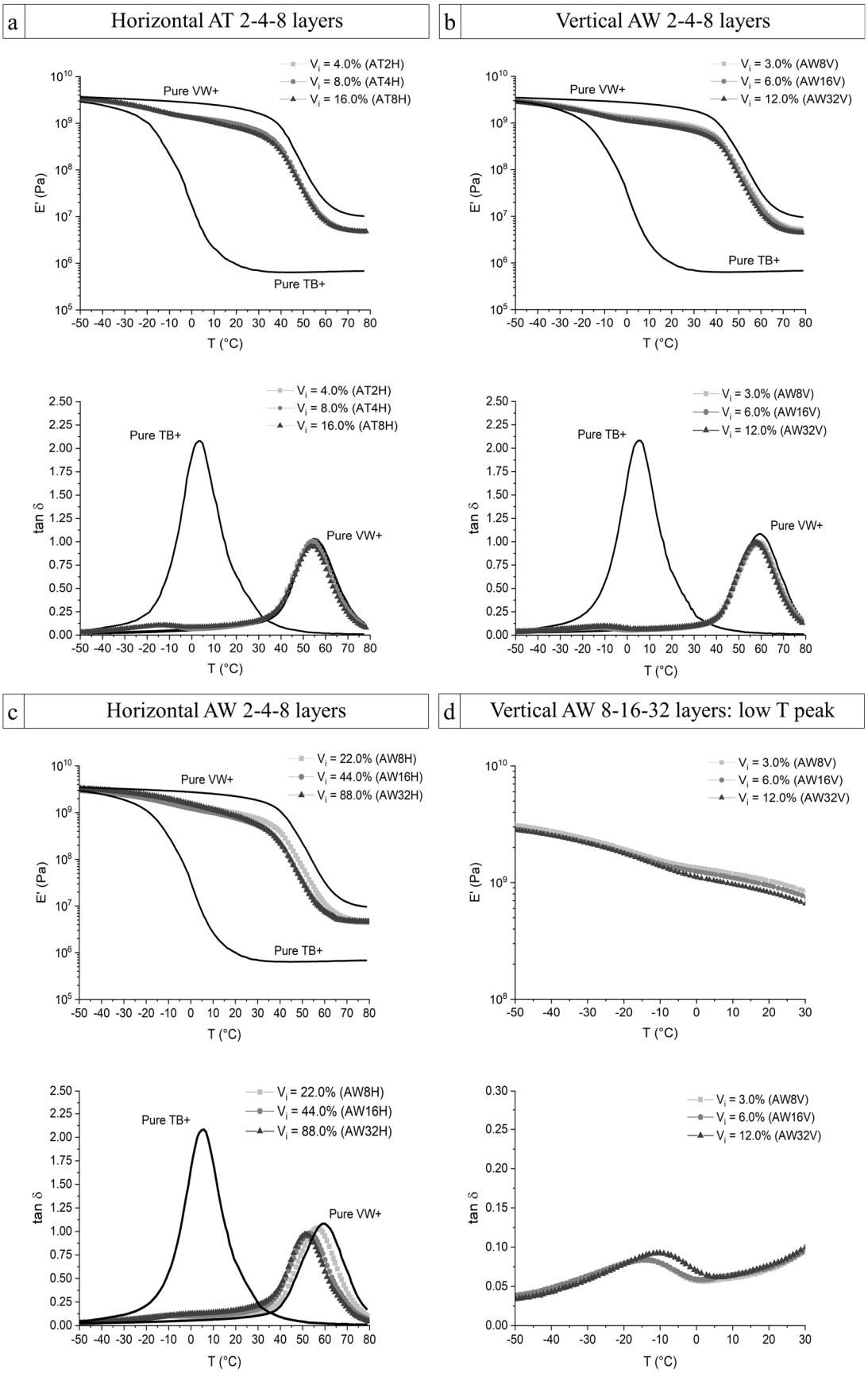

Figure 7. Storage modulus (top) and loss factor (bottom) of pure VW+, pure TB+ (continuous lines) and composite samples, labelled according to the corresponding nominal values of interphase volume fraction shown in Figure 4. The nomenclature used in the legend indicates: samples configuration (along width - AW or along thickness - AT), number of layers (2-32) and printing orientation (horizontal - H or vertical - V).

DMA data obtained on horizontally printed AT samples are reported in Figure 7a. As expected, intermediate storage modulus values between those of pure VW+ and TB+ were obtained, in agreement with the nominal 50-50 ratio employed for all composites. In this case a sharp interface is formed between adjacent layers; despite its larger surface (about 350 mm^2, as opposed to about 70 mm^2 for AW configuration), estimated values of the total interphase volume do not exceed 16% of the overall sample volume. Accordingly, no significant effect of this variable (strictly associated to the number of layers) was observed. The same is true for loss factor data, in which curves for 2, 4 and 8 layers are almost identical. They are very similar to the reference VW+ curve, with a main loss peak shifted by only a few degrees towards lower temperatures, a fact that can be easily explained assuming a predominantly glassy (i.e., akin to that of VW+) behaviour of the interface but allowing for a limited miscibility of the rubbery TB+ phase; this result is in accordance with previous findings [23]. A closer inspection of the loss factor curves for the AT composites reveals an additional peak, located at about -11°C, in place of the main TB+ one at 6°C which is almost completely suppressed in the composites. Its nature will be discussed later, once the results for the composite materials with higher TB+ content will be presented.

DMA scans of vertically printed AW samples are reported in Figure 7b. Also in this case formation of a sharp interface is expected. While its area is smaller, compared to AT configuration, the increased number of layers brings about a total interface volume of 12%, which is comparable to that of horizontally printed AT samples, as visible from Figure 4. Accordingly, DMA results are similar for the two cases: again, no evident effect of the (relatively limited) interphase volume fraction is apparent in the data with the curves corresponding to 8, 16 and 32 layers being practically superimposed.

To explore the behaviour of composites having a very high volume fraction of interphase, horizontally printed AW samples were investigated. Again, the number of layers was set at 8, 16 and 32. In particular the 32-layer configuration was designed to be constituted almost completely by interphase: the layer thickness in this case (170 μm) practically coincides with the estimated dimension for the blurred interface (~ 150 μm) [23]. This coincidence was exploited in the model presented later in this paper, by assuming the behaviour of this particular material to representative of the blurred interface. Relevant results are shown in Figure 7c. At variance with those obtained at lower interphase content, an effect of its volumetric fraction is visible: the storage modulus in the transition region is appreciably lower for the high-volume interphase samples (16 and 32 layers, whose V_i is 44% and 88%, respectively). In a similar way, the main loss factor peak for 16- and 32-layers horizontally printed AW samples is further shifted towards a lower temperature (about 50°C) with respect to the rest of the data. These results support the assumption that the material of the 32-layer samples is entirely made up of blurred interphase, whose behaviour is very close to that of VW+ alone; the slight reduction observed in the glass transition temperature is justified by the high content (50%) of TB+ in this monophasic blend, which yet remains glassy at room temperature. A qualitatively similar behaviour was observed in our previous work when considering samples with a layer thickness comparable to interphase dimension [23].

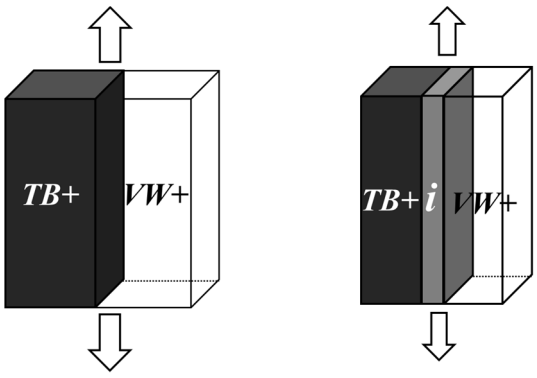

Figure 8. Analog models based on the rule of mixture for parallel configuration composites: without (left) and with (right) the explicit presence of the interphase.

To improve understanding of the data, measured properties were compared by considering the constituents of the specimen in a parallel configuration, with and without the explicit presence of a third interphase in addition to the two main VW+ and TB+ phases (see Figure 8). Assuming DMA results obtained on pure VW+ and TB+ (continuous curves in Figure 7) as reference values for the two constituents, the corresponding composite apparent elastic modulus and loss factor were computed for each temperature as the weighted average of the in-phase and out-of-phase components *E'* and *E''*:

$$E' = \sum_n v_n E'_n \quad [1]$$

$$E'' = \sum_n v_n E''_n \quad [2]$$

$$tan\delta = \frac{E''}{E'} = \frac{\sum_n v_n tan\delta_n E'_n}{\sum_n v_n E'_n} \quad [3]$$

in which v_n, E'_n and E''_n are the volume fraction, storage and loss modulus and $tan\delta_n = \frac{E''_n}{E'_n}$ is the loss factor of the n_{th} phase.

As previously mentioned, the effective properties of the interphase were taken from the results of the 32-layer horizontally printed AW material, which had interphase content highly predominant over pure TB+ and VW+ phases.

Predictions of the model were compared with relevant experimental data. Figure 9 shows model results for 8- and 16- layers horizontally printed AW samples, whose estimated volume fraction of (blurred) interphase is equal to 22% and 44%, respectively. Considering first a simpler model, corresponding to a sequence of pure alternating layers (of VW+ or TB+) with an ideal, zero-thickness interface, predicted values of the storage modulus are much higher than experimental ones in the main glass transition region, especially for the sample with $V_i = 44\%$. In turn, the model explicitly considering the presence of the interphase volume fraction provides a much better agreement with the experimental data. This observation is quantitatively supported by root mean square error (RMS) evaluation of *log E' vs. T* data performed in both cases, which is reduced by 40% for the model with the interphase (Figure 10). The comparison of predicted vs. experimental loss factor curves gives similar results, with the interphase model being more accurate especially at high interphase volume fraction. In particular at room temperature the more refined model is always closer to the experiments than its simpler version (Figure 10).

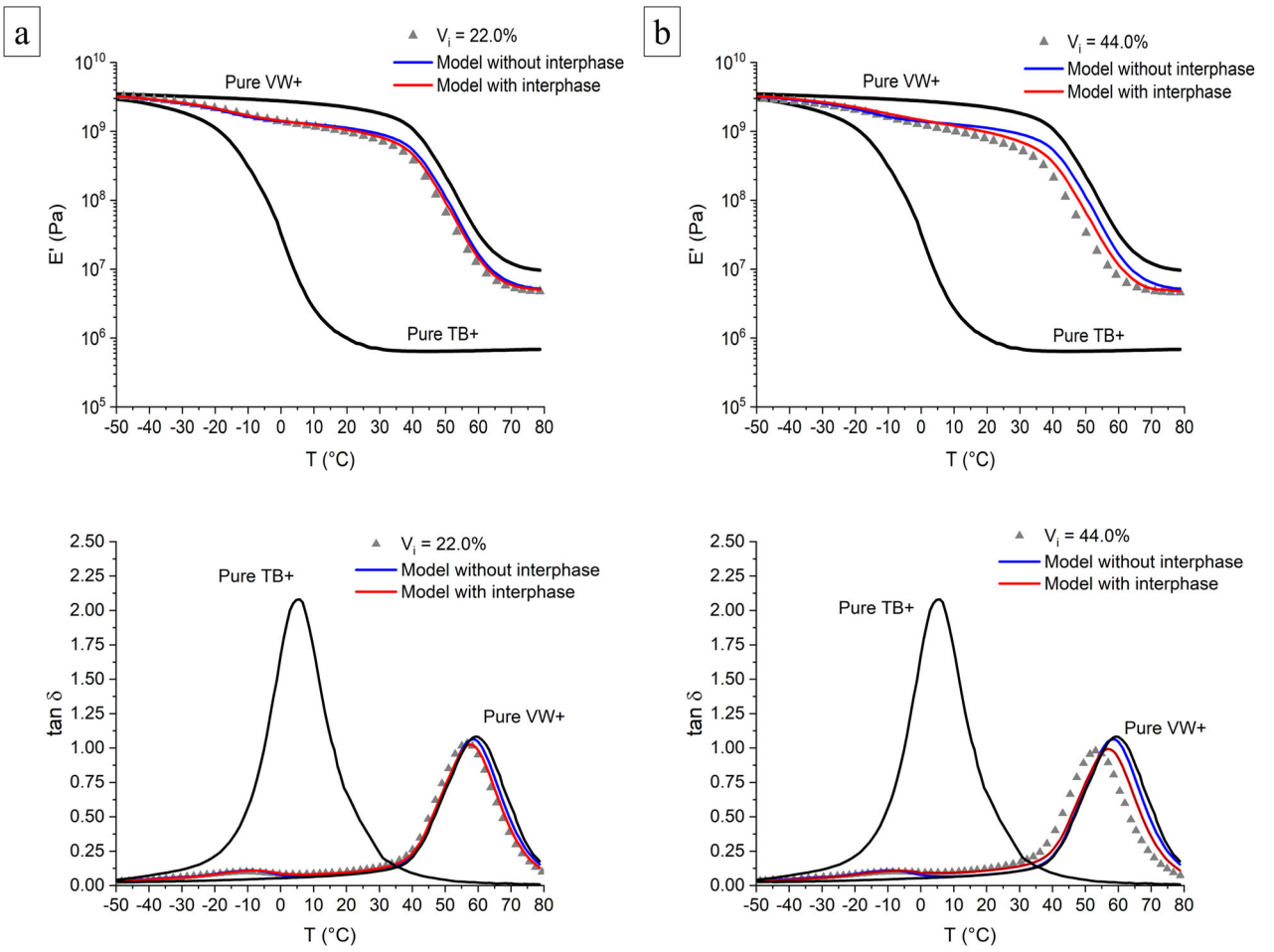

Figure 9. Comparison between experimental data and model predictions for modulus (top) and loss factor (bottom), with and without interphase, for a) 8- and b) 16- layers horizontally printed AW samples. Samples are labelled according to the theoretical interphase volume fraction.

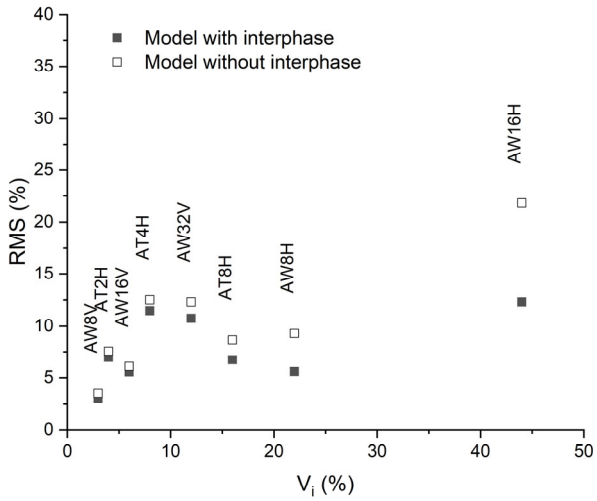

Figure 10. RMS comparison between model prediction and experimental logE' data for all tested samples, considering and neglecting the interphase.

It is worth observing that the real situation is obviously more complicated than the idealized distinction between the two constituent materials and a “pure” interphase, because interdiffusion among the different phases will result in a graded material. The description of a graded region would require a certain number of additional parameters whose identification poses quite a challenge [28]. Nevertheless, the proposed simplified approach succeeds in giving accurate predictions, at the same time demonstrating how the presence of a blurred interphase between the two pure phases should be considered in view of a correct evaluation of the final composite properties.

Considering the extensive usage of multimaterial Polyjet printing and the increasing interest in optimizing and predicting the behaviour of the printed composites with the support of numerical models [15,29,33,34] our results demonstrate that neglecting the presence of a significant fraction of interphase will inevitably affect the accuracy of these predictions. If this is true for the (visco)elastic properties considered so far, it is likely to become even more important when considering more localized phenomena such as yielding and fracture processes [28,30,35].

The final set of results considered in the present work concerns the effect of the material composition. Dynamic mechanical behaviour of samples having an unbalanced composition (in terms of the two constituents) ranging up to 95% TB+ was investigated; TB+ content lower than 50% was not considered since the 50:50 samples already demonstrated a behaviour close to the one of the pure glassy polymer. Data shown in Figure 11a display a quite obvious trend, with the storage modulus of composites with increasing fraction of TB+ steadily approaching the values of the reference pure material. However, the shape of the curves is different and it is interesting to look at loss factor data (Figure 11b) to analyse the two distinct loss peaks so far reported for many composite materials (Figure 7). As soon as the TB+ volume fraction increases above 50%, their characteristic low-temperature loss peak at about -11°C appears. Such low temperature transition was clearly observed in the multilayer samples as well as in the pure TB+ when tested in three-point-bending [23]. The peak amplitude progressively increases and it shifts towards higher temperatures with increasing TB+ content, although even at a value as high as 95%, the amplitude is still nearly an order of magnitude less than the corresponding pure TB+ value: even a very small fraction of VW+ aligned with the loading direction can be very effective in suppressing viscoelastic dissipation of the composites. Considering the “glassy” high temperature peak at about 59°C, it remains substantially unaffected by an increasing content of TB+ until the highest value considered (95%) is reached. At this stage, the nominal amount of pure VW+ phase left is only 5%, as the remaining volume is almost completely taken up by the interphase. When this occurs, the peak shifts towards lower temperatures.

Figure 11 shows also the prediction of the parallel model presented earlier. Although the interphase volumetric fraction is rather small in this case (about 4%), the generally more accurate version accounting for its presence was used. The model well captures the reported trends generated by the increase in TB+ content, although the accuracy of its prediction decreases especially for the highest value of 95%. With such high a volume of rubbery phase, discrepancy may be expected because of a generalized loss of constraint (away from the rigid glassy or inter-phases) in the experiment.

It is worth noticing that the model predicts the slight reduction of the low-temperature loss peaks in the composite compared to that of pure TB+. This result is a direct consequence of considering a parallel model to obtain both storage and loss moduli of the composite and agrees with findings obtained by Dickie [36], who analysed composite structures having a rigid continuous matrix and soft dispersed particles by developing an equivalent mechanical model based on the Kerner equation. Depending on the ratio between the storage moduli of the two phases, the author showed that indeed a shift of the loss peak of the dispersed soft phase towards lower temperatures is expected, which becomes larger with decreasing soft phase volume content. Although the multilayer composites characterized here are not traditional matrix-inclusion systems, their dynamic mechanical behaviour show some analogy with the composites therein described. Accordingly, the observed

loss peak should be considered as emerging from the complex dynamic interaction between the two phases rather than being representative of the TB+ glass transition.

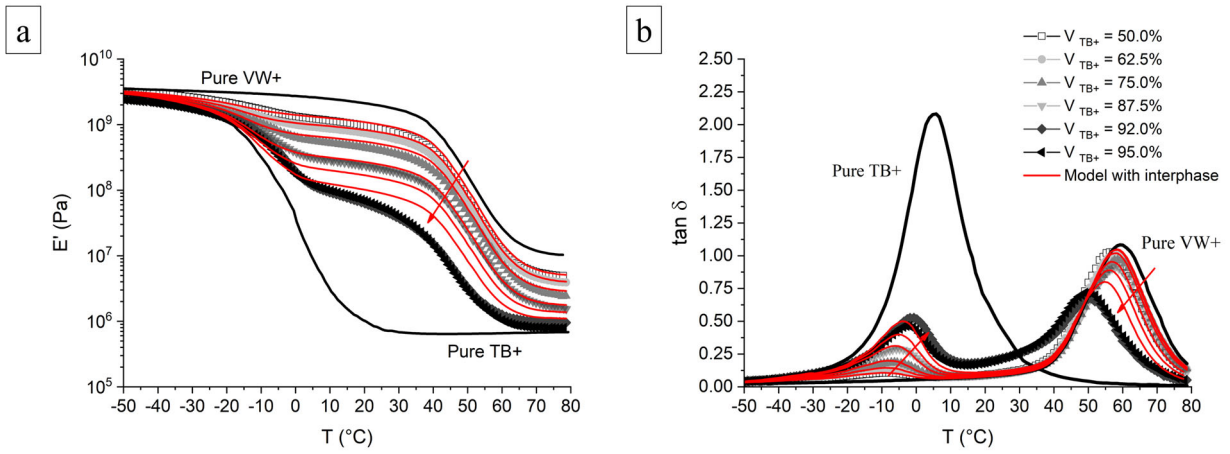

Figure 11. Storage modulus vs temperature (a) and loss factor vs temperature (b) curves of samples with increasing volumetric fraction of TB+ (from 50% up to 95%) compared to pure TB+ and VW+ behaviour (black continuous lines). The red lines represent the behaviour according to the model taking into account the presence of the interphase; arrows represent the variation of the model prediction with the increasing volume fraction of TB+.

5. Conclusions

This study explored the role of the interphase in 3D printed composites (fabricated via Polyjet technology) through tensile (dynamic) mechanical analysis performed on composite samples, prepared by stacking an equal number of layers made of two different polymers (one rubbery and the other glassy at room temperature) in various spatial configurations. The selected loading condition is favourable because a uniform stress state is enforced on every single layer, thus allowing the application of a very simple parallel model whose output was later compared with experimental results.

Firstly, we showed that the intrinsic variability in the mechanical behaviour of nominally identical 3D printed samples can be imputed to incomplete curing and such variability can be reduced by a proper thermal treatment.

It was found that for relatively low volume contents of interphase (below 20%) its presence could be neglected, since the samples substantially behave like the ideal bi-material composite they are meant to represent, with no or very little effect of the number and spatial arrangement of the different material layers. Conversely, when the volume fraction of the interphase is further increased because of the high number of layers and/or of the specific printing orientation, a clear effect can be observed. In fact, the interphase represents in this case a third constituent material whose behaviour is demonstrated to be quite similar to that of the base glassy polymer.

This was justified by a further study in which the composition of the samples was altered to include progressively larger fractions of the rubbery material. Results clearly showed that even modest volume fractions of the rigid glassy polymer (less than 10%) are sufficient to obtain an overall behaviour which substantially deviates from that of the pure rubbery constituent.

The model predictions compared well with all the previous findings. Interphase properties were determined by analysing many-layered samples which were almost completely made up of this third constituent. Two variants were considered, with and without the explicit presence of the interphase. While the two agree well for low

interphase content, the superiority of the model which also includes it was clearly demonstrated in the case of higher values.

The results provided by the present investigation are of great importance for the purpose of modelling the behaviour of complex co-continuous architectures (such as Interpenetrating Phase Composites) which are often seen as a way to create bio-inspired materials with tuneable properties. Due to the typically very large interface area generated in these structures, a strong influence of interphase properties is expected and the models used for their optimization need to take it into account. These findings, which are already significant when considering the small-strain (visco)elastic behaviour of co-continuous composites, may become critical if larger deformations are involved: the associated phenomena (namely yielding and fracture) are often very localized and may be dominated by the characteristics of the interphase.

6. Acknowledgments

We would like to thank Stefano Tagliabue from Politecnico di Milano for the help during the tests and Quentin Grossman from ULiege for printing some of the samples used in this work.

References

[1] Studart AR. Additive manufacturing of biologically-inspired materials. Chem Soc Rev 2016;45:359–76. https://doi.org/10.1039/c5cs00836k.

[2] Ge C, Cormier D, Rice B. Damping and cushioning characteristics of Polyjet 3D printed photopolymer with Kelvin model. J Cell Plast 2021;57:517–34. https://doi.org/10.1177/0021955X20944972.

[3] Ngo TD, Kashani A, Imbalzano G, Nguyen KTQ, Hui D. Additive manufacturing (3D printing): A review of materials, methods, applications and challenges. Compos Part B Eng 2018;143:172–96. https://doi.org/10.1016/j.compositesb.2018.02.012.

[4] Ligon SC, Liska R, Stampfl J, Gurr M, Mülhaupt R. Polymers for 3D Printing and Customized Additive Manufacturing. Chem Rev 2017;117:10212–90. https://doi.org/10.1021/acs.chemrev.7b00074.

[5] Bandyopadhyay A, Heer B. Additive manufacturing of multi-material structures. Mater Sci Eng R Reports 2018;129:1–16. https://doi.org/10.1016/j.mser.2018.04.001.

[6] Velasco-Hogan A, Xu J, Meyers MA. Additive Manufacturing as a Method to Design and Optimize Bioinspired Structures. Adv Mater 2018;30. https://doi.org/10.1002/adma.201800940.

[7] Zorzetto L, Ruffoni D. Wood-Inspired 3D-Printed Helical Composites with Tunable and Enhanced Mechanical Performance. Adv Funct Mater 2019;29. https://doi.org/10.1002/adfm.201805888.

[8] Rafiee M, Farahani RD, Therriault D. Multi-Material 3D and 4D Printing: A Survey. Adv Sci 2020;7:1–26. https://doi.org/10.1002/advs.201902307.

[9] Libonati F, Gu GX, Qin Z, Vergani L, Buehler MJ. Bone-Inspired Materials by Design: Toughness Amplification Observed Using 3D Printing and Testing. Adv Eng Mater 2016;18:1354–63. https://doi.org/10.1002/adem.201600143.

[10] Kim Y, Kim Y, Libonati F, Ryu S. Designing tough isotropic structural composite using computation, 3D printing and testing. Compos Part B Eng 2019;167:736–45. https://doi.org/10.1016/j.compositesb.2019.03.039.

[11] Dunlop JWC, Fratzl P. Biological composites. Annu Rev Mater Res 2010;40:1–24. https://doi.org/10.1146/annurev-matsci-070909-104421.

[12] Porter MM, Ravikumar N, Barthelat F, Martini R. 3D-printing and mechanics of bio-inspired articulated and multi-material structures. J Mech Behav Biomed Mater 2017;73:114–26. https://doi.org/10.1016/j.jmbbm.2016.12.016.

[13] Meisel NA, Dillard DA, Williams CB. Impact of material concentration and distribution on composite parts manufactured via multi-material jetting. Rapid Prototyp J 2018;24:872–9. https://doi.org/10.1108/RPJ-01-2017-0005.

[14] Hofmann M. 3D printing gets a boost and opportunities with polymer materials. ACS Macro Lett 2014;3:382–6. https://doi.org/10.1021/mz4006556.

[15] Wang L, Lau J, Thomas EL, Boyce MC. Co-continuous composite materials for stiffness, strength, and energy dissipation. Adv Mater 2011;23:1524–9. https://doi.org/10.1002/adma.201003956.

[16] Feng XQ, Mai YW, Qin QH. A micromechanical model for interpenetrating multiphase composites. Comput Mater Sci 2003;28:486–93. https://doi.org/10.1016/j.commatsci.2003.06.005.

[17] Al-Ketan O, Al-Rub RKA, Rowshan R. Mechanical Properties of a New Type of Architected Interpenetrating Phase Composite Materials. Adv Mater Technol 2017;2:1–7. https://doi.org/10.1002/admt.201600235.

[18] Dalaq AS, Abueidda DW, Abu Al-Rub RK. Mechanical properties of 3D printed interpenetrating phase

composites with novel architectured 3D solid-sheet reinforcements. Compos Part A Appl Sci Manuf 2016;84:266–80. https://doi.org/10.1016/j.compositesa.2016.02.009.

[19] Al-Ketan O, Adel Assad M, Abu Al-Rub RK. Mechanical properties of periodic interpenetrating phase composites with novel architected microstructures. Compos Struct 2017;176:9–19. https://doi.org/10.1016/j.compstruct.2017.05.026.

[20] Al-Ketan O, Soliman A, AlQubaisi AM, Abu Al-Rub RK. Nature-Inspired Lightweight Cellular Co-Continuous Composites with Architected Periodic Gyroidal Structures. Adv Eng Mater 2018;20. https://doi.org/10.1002/adem.201700549.

[21] Miserez A, Schneberk T, Sun C, Zok FW, Waite JH. The transition from stiff to compliant materials in squid beaks. Science (80-) 2008;319:1816–9. https://doi.org/10.1126/science.1154117.

[22] Tumbleston JR, Shirvanyants D, Ermoshkin N, Janusziewicz R, Johnson AR, Kelly D, et al. Continuous liquid interface production of 3D objects. Science (80-) 2015;347:1349–52. https://doi.org/10.1126/science.aaa2397.

[23] Zorzetto L, Andena L, Briatico-Vangosa F, De Noni L, Thomassin JM, Jérôme C, et al. Properties and role of interfaces in multimaterial 3D printed composites. Sci Rep 2020;10:1–17. https://doi.org/10.1038/s41598-020-79230-0.

[24] Dimas LS, Bratzel GH, Eylon I, Buehler MJ. Tough composites inspired by mineralized natural materials: Computation, 3D printing, and testing. Adv Funct Mater 2013;23:4629–38. https://doi.org/10.1002/adfm.201300215.

[25] Ivan Vu; Lindsey Bass; Nicholas Meisel, Bruce Orler, Christopher B. Williams DAD. Characterization of Mutli-Material Interfaces in PolyJet Additive Manufacturing. Solid Free Fabr Symp Proc 2014:959–82.

[26] Dolinski ND, Callaway EB, Sample CS, Gockowski LF, Chavez R, Page ZA, et al. Tough Multimaterial Interfaces through Wavelength-Selective 3D Printing. ACS Appl Mater Interfaces 2021;13:22065–72. https://doi.org/10.1021/acsami.1c06062.

[27] Kuang X, Wu J, Chen K, Zhao Z, Ding Z, Hu F, et al. Grayscale digital light processing 3D printing for highly functionally graded materials. Sci Adv 2019;5:1–10. https://doi.org/10.1126/sciadv.aav5790.

[28] Liu F, Li T, Jiang X, Jia Z, Xu Z, Wang L. The effect of material mixing on interfacial stiffness and strength of multi-material additive manufacturing. Addit Manuf 2020;36. https://doi.org/10.1016/j.addma.2020.101502.

[29] Mueller J, Shea K, Daraio C. Mechanical properties of parts fabricated with inkjet 3D printing through efficient experimental design. Mater Des 2015;86:902–12. https://doi.org/10.1016/j.matdes.2015.07.129.

[30] Mueller J, Courty D, Spielhofer M, Spolenak R, Shea K. Mechanical Properties of Interfaces in Inkjet 3D Printed Single- and Multi-Material Parts. 3D Print Addit Manuf 2017;4:193–9. https://doi.org/10.1089/3dp.2017.0038.

[31] Ge Q, Dunn CK, Qi HJ, Dunn ML. Active origami by 4D printing. Smart Mater Struct 2014;23. https://doi.org/10.1088/0964-1726/23/9/094007.

[32] Yuan C, Wang F, Rosen DW, Ge Q. Voxel design of additively manufactured digital material with customized thermomechanical properties. Mater Des 2021;197. https://doi.org/10.1016/j.matdes.2020.109205.

[33] Zhang P, Heyne MA, To AC. Biomimetic staggered composites with highly enhanced energy dissipation: Modeling, 3D printing, and testing. J Mech Phys Solids 2015;83:285–300. https://doi.org/10.1016/j.jmps.2015.06.015.

[34] Zorzetto L, Ruffoni D. Re-entrant inclusions in cellular solids: From defects to reinforcements. Compos Struct 2017;176:195–204. https://doi.org/10.1016/j.compstruct.2017.05.039.

[35] Li T, Chen Y, Wang L. Enhanced fracture toughness in architected interpenetrating phase composites by 3D printing. Compos Sci Technol 2018;167:251–9. https://doi.org/10.1016/j.compscitech.2018.08.009.

[36] Dickie RA. Heterogeneous polymer–polymer composites. I. Theory of viscoelastic properties and equivalent mechanical models. J Appl Polym Sci 1973;17:45–63. https://doi.org/10.1002/app.1973.070170104.